Electronic Supplementary Material (ESI) for Journal of Materials Chemistry B.
This journal is © The Royal Society of Chemistry 2024

Electronic Supplementary Information

Tough and elastic hydrogels based on robust hydrophobicity-assisted metal ion coordination for flexible wearable devices

Zheng Liu,‡[a] Kaixiang Shen,‡[a] Mengyuan Zhang,[a] Yuchen Zhang,[b] Zhuting Lv,[a] Qinghua Shang,[a] Renjie Li,[a] Can Zhou*[c] and Yilong Cheng*[ad].

[a] Engineering Research Center of Energy Storage Materials and Devices, Ministry of Education, School of Chemistry, Xi'an Jiaotong University, Xi'an 710049, China.

[b] Key Laboratory of Shaanxi Province for Craniofacial Precision Medicine Research, College of Stomatology, Xi'an Jiaotong University, Xi'an 710049, China.

[c] Breast Surgery Department, First Affiliated Hospital, Xi'an Jiaotong University, Xi'an 710049, China.

[d] Department of Nuclear Medicine, the First Affiliated Hospital of China, Xi'an Jiaotong University, Xi'an 710049, China.

* E-mail: yilongcheng@mail.xjtu.edu.cn;

E-mail: zhoucanz2005@126.com.

‡ These authors contributed equally to this work.

Experimental

Materials

Acrylamide (AM) was sourced from Adamas-beta Co., Ltd. Zirconyl chloride octahydrate ($ZrOCl_2 \cdot 8H_2O$) was acquired from Shanghai Aladdin Bio-Chem Technology Co., Ltd. 2-Hydroxy-4'-(2hydroxyethoxy)-2-methylpropiophenone (2959) was obtained from Shanghai Macklin Biochemical Co., Ltd. All reagents and chemicals used were of analytical purity. Deionized water, prepared in-house, was utilized in all experiments. N-Acryloyl glycine (AG)/N-acryloyl alanine (AA)/N-acryloyl valine (AV) was synthesized following established protocols as detailed in previous work[1], and the monomers were characterized by NMR (Fig S1-S3).

Computational simulation

Utilizing the density functional theory (DFT) methodology,[2] specifically the ORCA 5.0 program with the B3LYP composite function[3] and def2-TZVP basis set,[4] structural optimization and frequency calculations were performed on coordination complexes formed by AG/AA/AV with Zr^{4+}. Subsequently, the ORCA 5.0 program was combined with the doubly hybrid functional PWPB95[5] and the def2-QZVPP basis set[6] to compute the binding energy (ΔE) of the coordination complexes, with due consideration given to the basis set superposition error (BSSE).[7,8] The ΔE was calculated with Eq. (1):

$$\Delta E = E_{complex} - E_{Zr^{4+}} - E_{ligand} + E_{BSSE} \quad (1)$$

where $E_{complex}$, E_{Zr4+}, E_{ligand} and E_{BSSE} are energies of the coordination complex, Zr^{4+}, ligand and error correction, respectively.

Preparation of P(AM-AG/AA/AV)-Zr^{4+} hydrogels

The hydrogels were synthesized using a one-step free radical polymerization method. Initially, transparent aqueous solutions of the precursors were prepared by AM, AG/AA/AV, $ZrOCl_2 \cdot 8H_2O$, and 2959 in DI water. Subsequently, the precursor solution was transferred to a reaction cell assembled from a pair of glass plates and a silica sheet. The assembly was then irradiated with 365 nm UV light for 30 min at room temperature

to initiate the polymerization reaction and produce the hydrogels.

2.4 Characterization

Fourier-transform infrared (FTIR, Nicolet iS50) and Raman (InVia Qontor) spectroscopy were employed to identify the characteristic functional groups presented in the hydrogels and to evaluate the coordination of metal ions. The structure and nature of the carboxyl-Zr^{4+} coordination bonds were elucidated using XPS (ESCALAB Xi+, ThermoFisher Scientific). Scanning electron microscopy (SEM, Gemini SEM 500) was utilized to observe the microstructure and surface morphology of the hydrogels. The dynamic rheological behavior of the samples was assessed using a rheometer (Anton Paar MCR302) featuring a rotor diameter of 15 mm. The rheological properties of the hydrogels were evaluated at room temperature, maintaining a fixed strain of 1% and an angular frequency of 1 Hz throughout the testing period.

2.5 Swelling behavior

The initial mass of the hydrogel in its original state was measured and denoted as W_0. Subsequently, the hydrogel was immersed in deionized water for varying durations. Upon completion of the swelling process, excess water on the hydrogel's surface was carefully removed using absorbent paper, after which the hydrogel was immediately re-weighed, yielding the mass (W_t). The swelling rate (SR) of hydrogel was then determined using the Eq. (2).

$$SR = \frac{W_t - W_0}{W_0} \times 100\% \tag{2}$$

2.6 Mechanical test

Tensile and compression tests were performed on hydrogels using an electromechanical tester (CMT1503) at room temperature to characterize mechanical properties. The samples for tensile tests were dumbbell-shaped (16×4×1 mm^3), and cylindrical samples (d=12 mm, h=10 mm) for compression tests. At least five samples of each hydrogel were tested. Uniaxial tensile tests were conducted using a 50 N load cell and a tensile rate of 50 mm/min. To prevent evaporation during cyclic tensile tests, silicone oil was applied to the surface of the hydrogel. The tensile strain was set to 30%,

and the tensile rate was maintained at 50 mm/min throughout the test. The energy dissipation was determined by calculating the area enclosed within the hysteresis loop. For the uniaxial compression test (95% compression strain), a 5000 N load cell was employed at a compression rate of 10 mm/min. Silicone oil was also applied to the hydrogel surface to prevent evaporation during the cyclic compression test. The compressive strain was set to 50%, and the compression rate was maintained at 10 mm/min throughout the test.

2.7 Tearing test

For the tear test, rectangular-shaped hydrogel samples were prepared with dimensions a_0=20 mm (length) and b_0=1 mm (width). These samples featured an initial notch of 8 mm. During the tear test, the tensile speed was maintained at 50 mm/min. The fracture energy (Γ) was determined using the Eq. (3).

$$\Gamma = \frac{U(L_c)}{a_0 b_0} \tag{3}$$

where $U(L_c)$ represents the integral area under the force-distance curve of the unnotched specimen at the critical distance L_c, while L_c is the critical displacement of notched samples when the notch becomes a working crack.

2.8 Electrical test

The conductivity (σ) of the hydrogels was determined using an electrochemical workstation (CHI650E). The electrochemical impedance spectra were acquired over a frequency range spanning from 10^{-1} to 10^{6} Hz with 10 mV voltage. The impedance values were calculated utilizing the Eq. (4).

$$\sigma = \frac{L}{RS} \tag{4}$$

where L is the distance between the electrode sheets, S refers to the cross-sectional area of the electrode sheets, and R is the resistance of the hydrogel.

The electrochemical workstation, in conjunction with an electromechanical tester, was employed to monitor the resistance change curve of the hydrogels under varying strains and pressures. A humidifier was utilized during the test to maintain consistent environmental humidity levels. As the hydrogel sensor underwent stretching or

compression, the aforementioned instruments recorded real-time changes in its resistance. The relative change in resistance ($\Delta R/R_0$) was calculated using the Eq. (5).

$$\frac{\Delta R}{R_0} = \frac{R - R_0}{R_0} \tag{5}$$

where R_0 represents the initial resistance of the hydrogel, and R represents the resistance measured after applying strain or pressure to the hydrogel.

The gauge factor (GF) was defined as:

$$GF = \frac{\Delta R/R_0}{\varepsilon} \tag{6}$$

The sensitivity (S) was defined as:

$$s = \frac{\Delta R/R_0}{\sigma} \tag{7}$$

2.9 Flexible wearable sensor application

An electrode-connected signal acquisition board and an oscilloscope (SDS6054 H10pro) comprised the signal acquisition system used for measuring electrophysiological signals. Human motion signals were detected by directly connecting the hydrogel to the human body. Real-time recording of resistance changes was performed using an electrochemical workstation.

2.10 Biocompatibility

The cytocompatibility of the hydrogels was assessed in *vitro* using the 3-(4,5-dimethyl-2-thiazolyl)-2,5-diphenyltetrazolium bromide (MTT) assay and live-dead cell staining methods. For the MTT assay, fibroblasts (L929) were initially cultured in DMEM supplemented with 10% fetal bovine serum (FBS) and 1% Penicillin-Streptomycin (Hyclone). The cells were then incubated in a standard cell culture incubator set to 37°C for 24 h. Following this, L929 cells were seeded into 96-well plates at a density of 2,000 cells per well. After 24 hours of cell adherence, the medium in each well was replaced with 100 μL of hydrogel extract at various concentrations. The cells were then further incubated for 1, 2, and 3 days. To assess cell viability, 20 μL of MTT solution was added to each well after the respective incubation periods, and

the plates were incubated for an additional 4 h. Subsequently, 100 μL of DMSO was added to each well to replace the medium and solubilize the formazan crystals formed by viable cells. The plates were then shaken for 15 min, and the absorbance of the formazan solution was measured at 570 nm using a Multiskan FC Microplate Reader (Thermo Fisher Scientific, USA). *Cell viability* was calculated using the Eq. (8).

$$Cell\ viability(\%) = \frac{A_e - A_b}{A_c - A_b} \times 100\% \tag{8}$$

where A_e, A_b, and A_c represent the absorbance values of the experimental group, background group, and blank group, respectively.

Cell live-dead staining experiments were conducted by initially seeding L929 cells at a density of 10000 cells per well in 24-well plates. The cells were then cultured in DMEM medium supplemented with 10% FBS and 1% penicillin-streptomycin for 24 h in a CO_2 incubator at 37 degrees Celsius. Subsequently, 500 μL of a 50 mg/mL hydrogel extraction solution was added to each well, and incubation was continued for 1, 2, and 3 days. Upon completion of the incubation period, the liquid was discarded, and 250 μL of a staining working solution was added to each well for 30 min. The staining working solution contained calcein, which stains live cells (492 nm, appearing green), and propidium iodide, which stains dead cells (545 nm, appearing red). The fluorescence of the stained cells was observed using a fluorescence microscope ((DMi8, Leica, Germany) to distinguish live and dead cells based on their respective fluorescence emission wavelengths.

Kunming mice (male, 6-8 weeks, 25-30g) were utilized to evaluate the histocompatibility of the hydrogels. These mice were procured from the Experimental Animal Center of Xi'an Jiaotong University. The animal protocols employed in this study received approval from the Ethics Committee of Xi'an Jiaotong University, ensuring compliance with ethical guidelines. All animal experiments adhered to the standards set forth by the Institutional Animal Care and Use Committee (IACUC) established by the Health Science Center of Xi'an Jiaotong University. Initially, the back of the anesthetized mice underwent local depilation and disinfection treatment. Subsequently, a hydrogel with a diameter of 5 mm and a thickness of 1 mm was

implanted into the mice following an incision of approximately 1 cm. Tissue samples were collected from the implantation site on days 3, 7, 14, and 28 post-implantation. The evaluation of tissue compatibility was conducted using hematoxylin and eosin (H&E) staining techniques.

2.11 Statement

Informed consent was obtained for the experiments involving human participants.

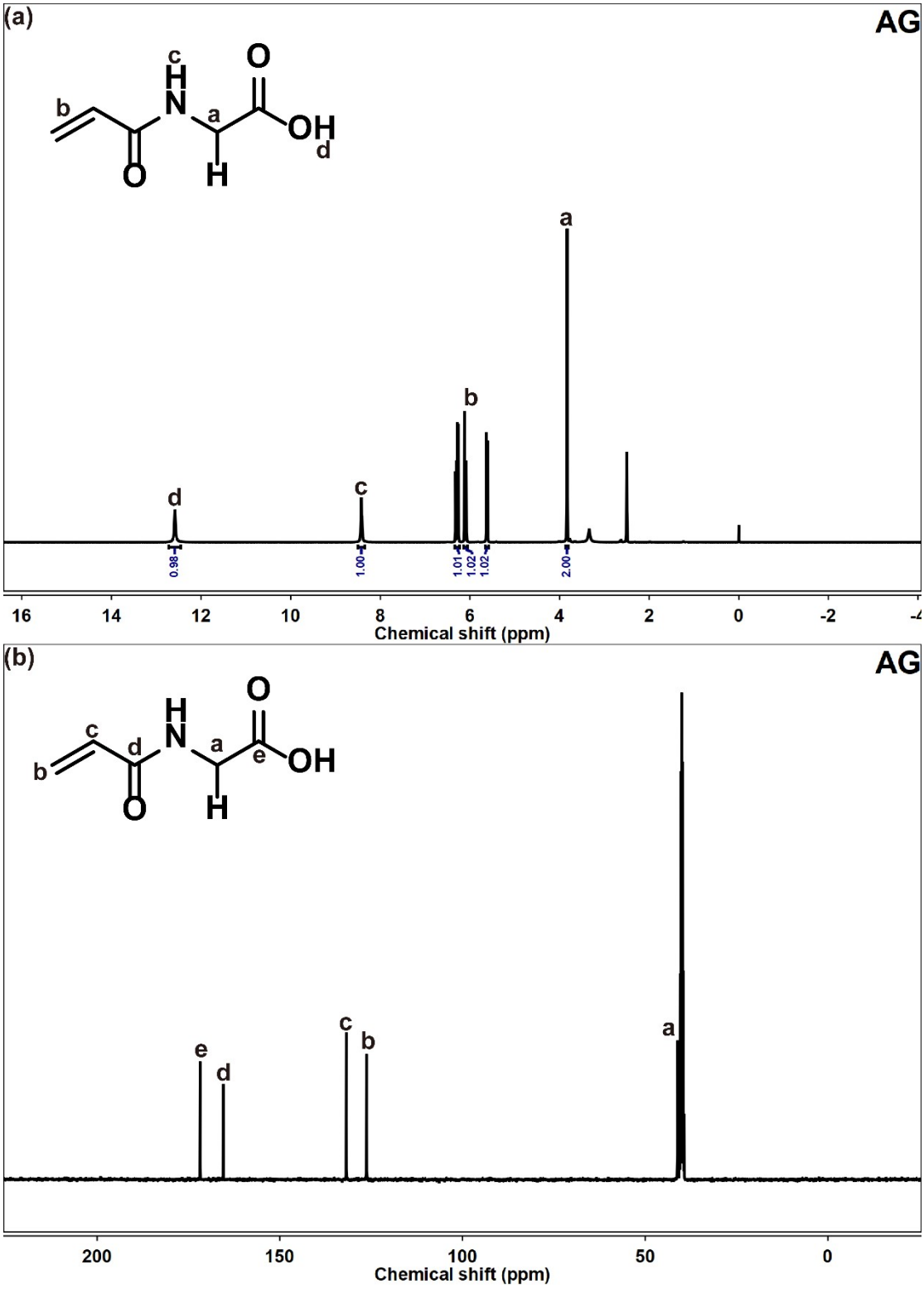

Fig. S1 ^{1}H (a) and ^{13}C (b) NMR spectra of N-acryloyl glycine (AG) in DMSO-d6.

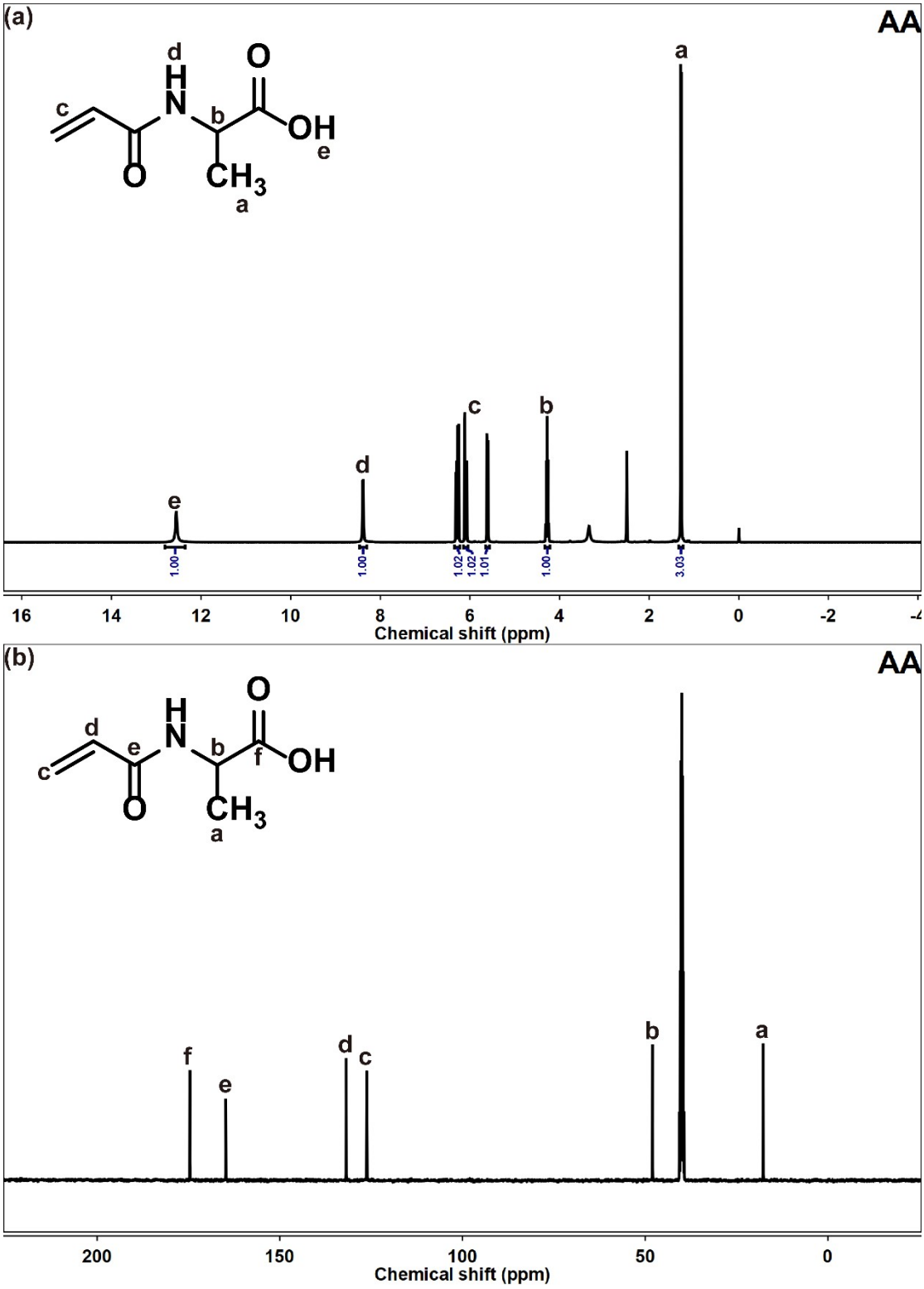

Fig. S2 ^{1}H (a) and ^{13}C (b) NMR spectra of N-acryloyl alanine (AA) in DMSO-d6.

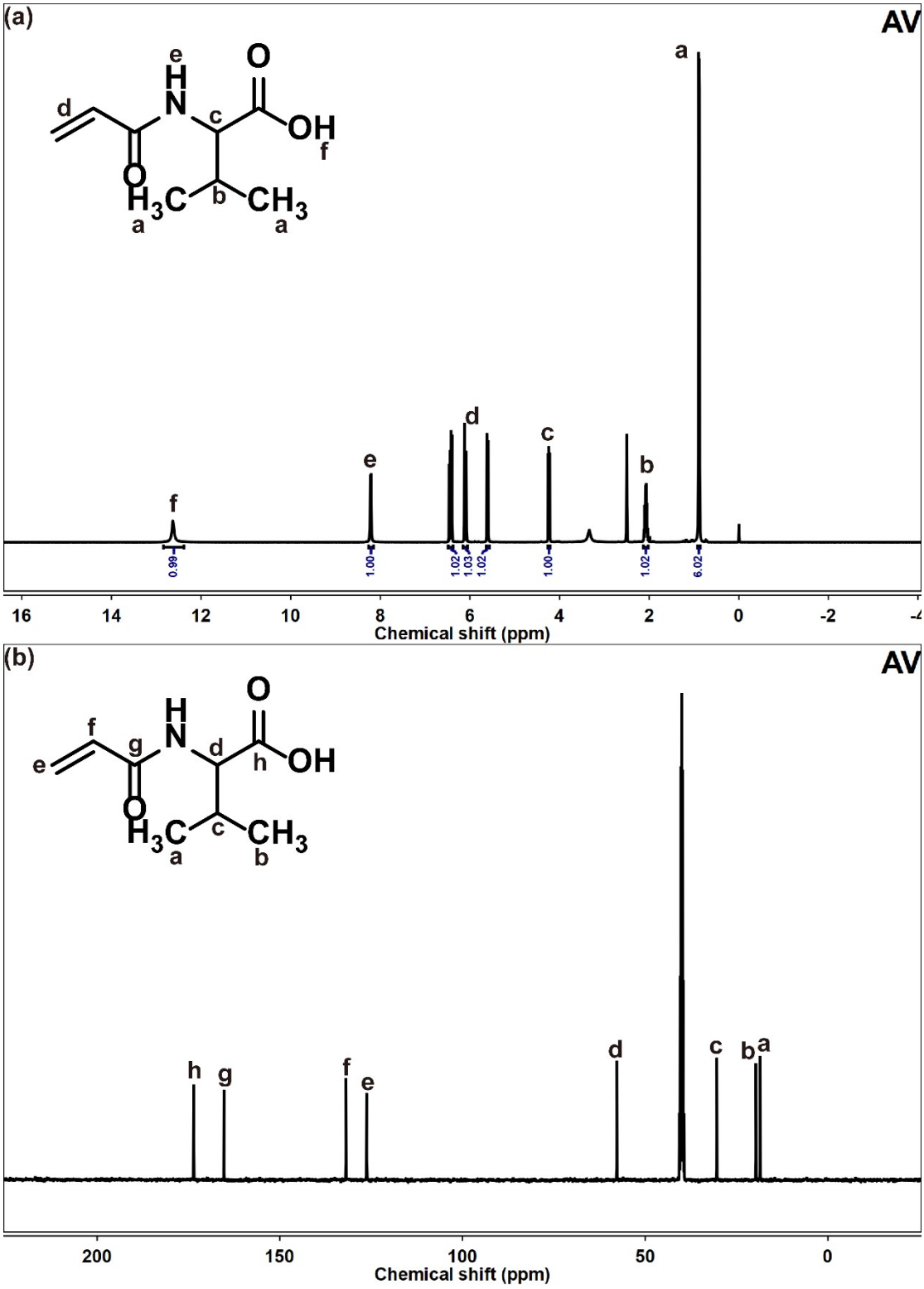

Fig. S3 ^{1}H (a) and ^{13}C (b) NMR spectra of N-acryloyl valine (AV) in DMSO-d6.

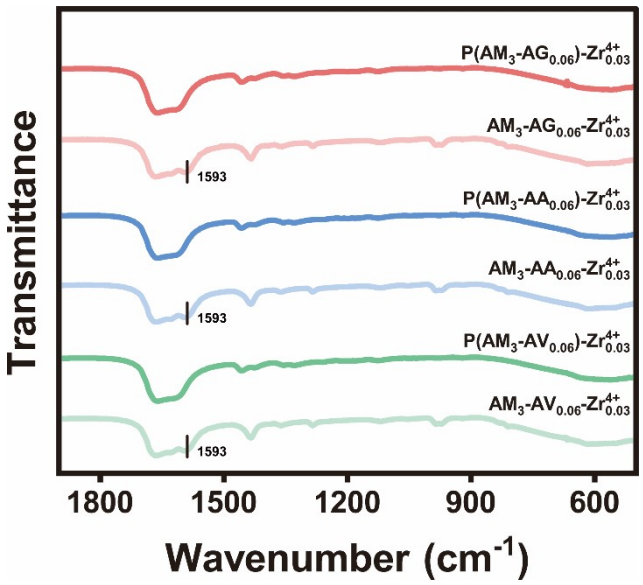

Fig. S4 FTIR spectra of precursors and hydrogels.

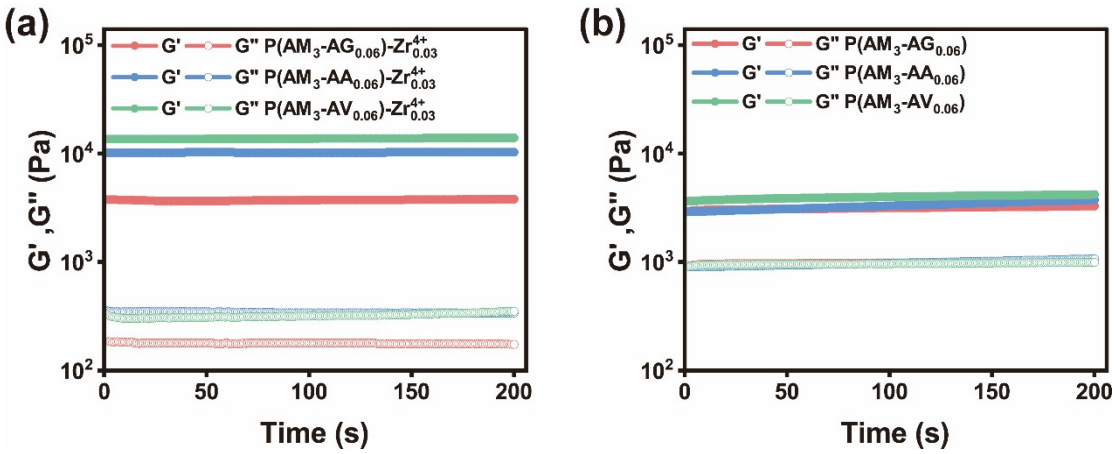

Fig. S5 Rheological characterization of P(AM_3-AG/AA/$AV_{0.06}$) and P(AM_3-AG/AA/$AV_{0.06}$)-Zr4+ 0.03 hydrogels.

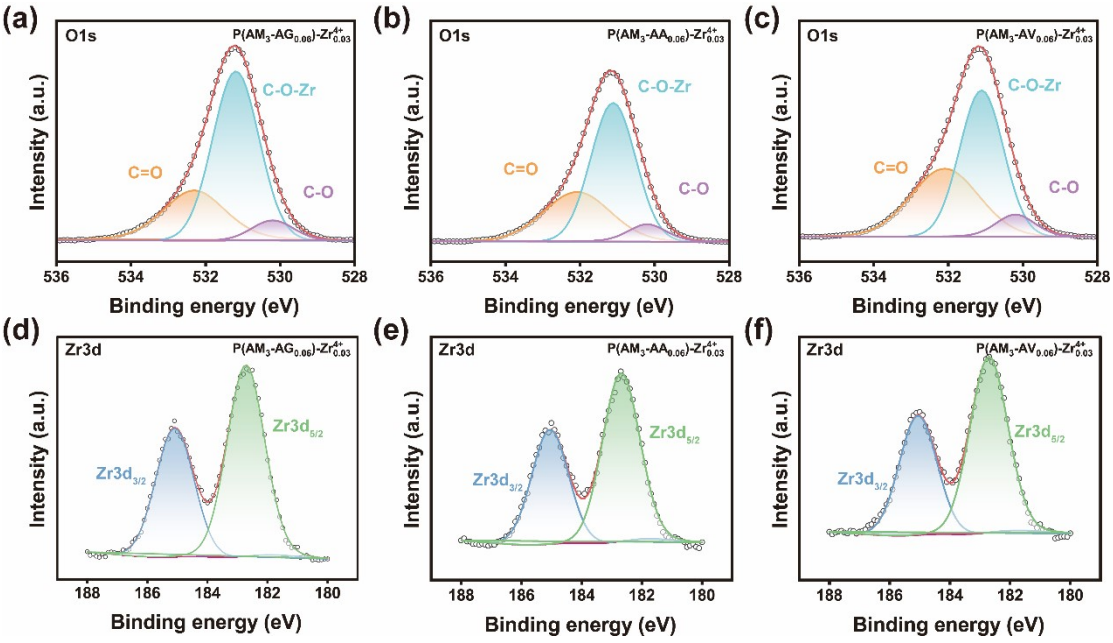

Fig. S6 High-resolution XPS spectra of deconvoluted O 1s (a-c) and Zr 3d (d-f) orbits of the P(AM_3-AG/AA/$AV_{0.06}$)-Zr4+ 0.03 hydrogels.

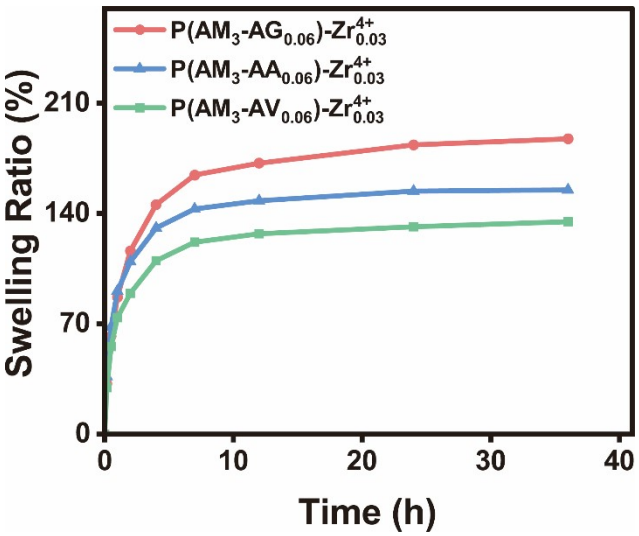

Fig. S7 Dynamic swelling curves of P(AM_3-AG/AA/$AV_{0.06}$)-Zr4+ 0.03 hydrogels.

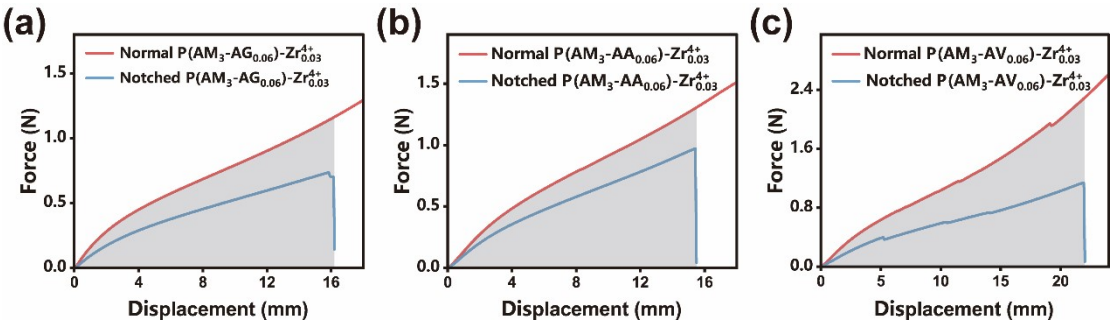

Fig. S8 The force-displacement curves of the notched and unnotched of $P(AM_3\text{-}AG_{0.06})$-Zr4+ 0.03 hydrogel (a), $P(AM_3\text{-}AA_{0.06})$-Zr4+ 0.03 hydrogel (b) and $P(AM_3\text{-}AV_{0.06})$-Zr4+ 0.03 hydrogel (c).

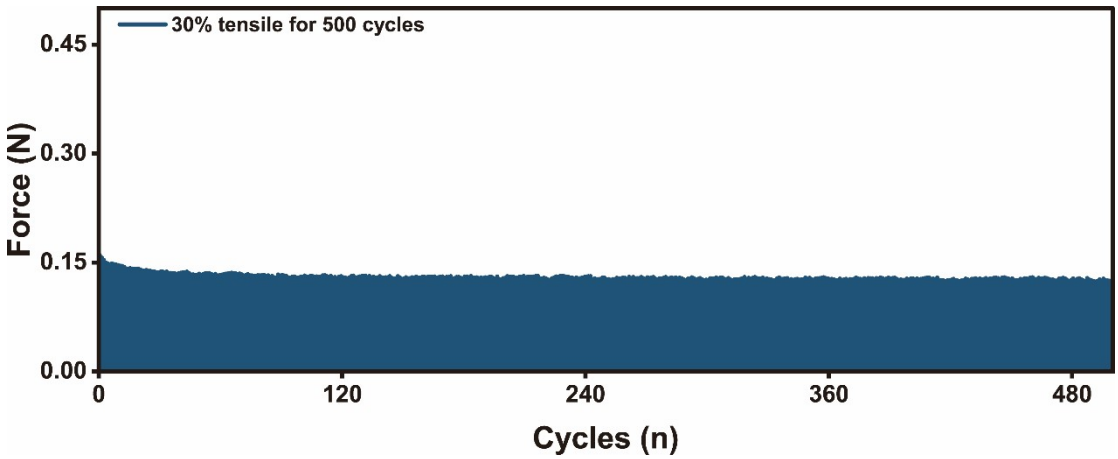

Fig. S9 Cyclic tensile mechanical properties of P(AM_3-$AV_{0.06}$)-Zr4+ 0.03 hydrogel.

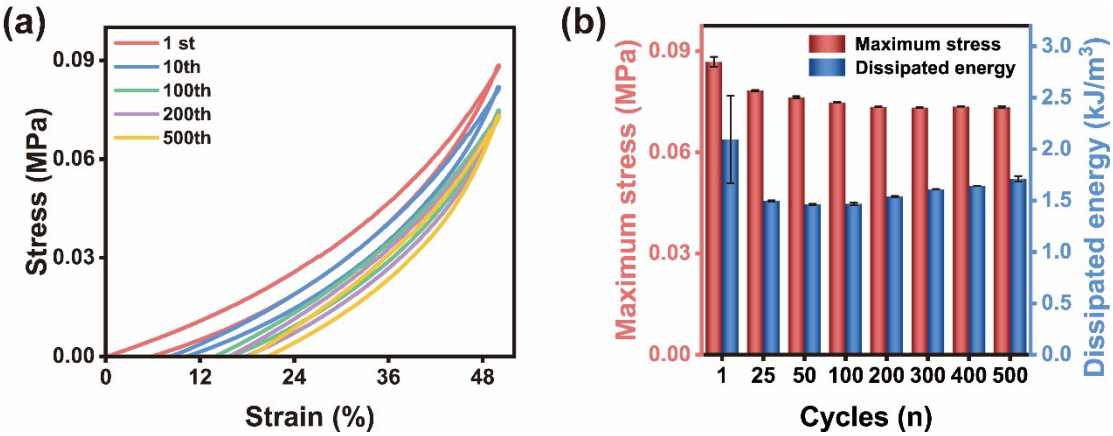

Fig. S10 Cyclic compression stress–strain curves (a) and corresponding mechanical properties (b) of P(AM_3-$AV_{0.06}$)-Zr4+ 0.03 hydrogel.

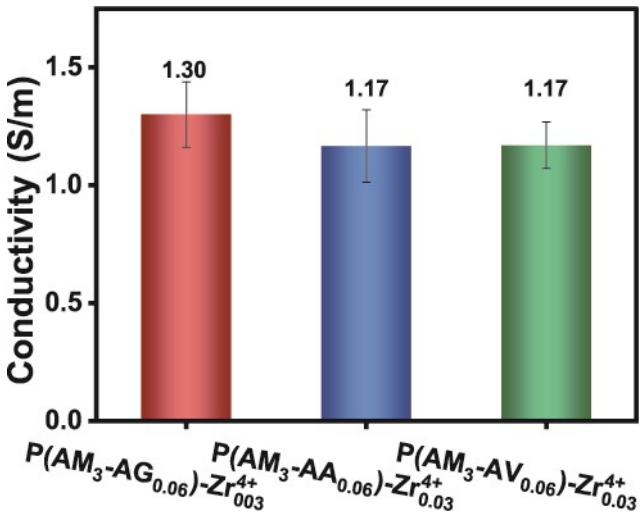

Fig. S11 Conductivity of P(AM_3-AG/AA/$AV_{0.06}$)-Zr4+ 0.03 hydrogels.

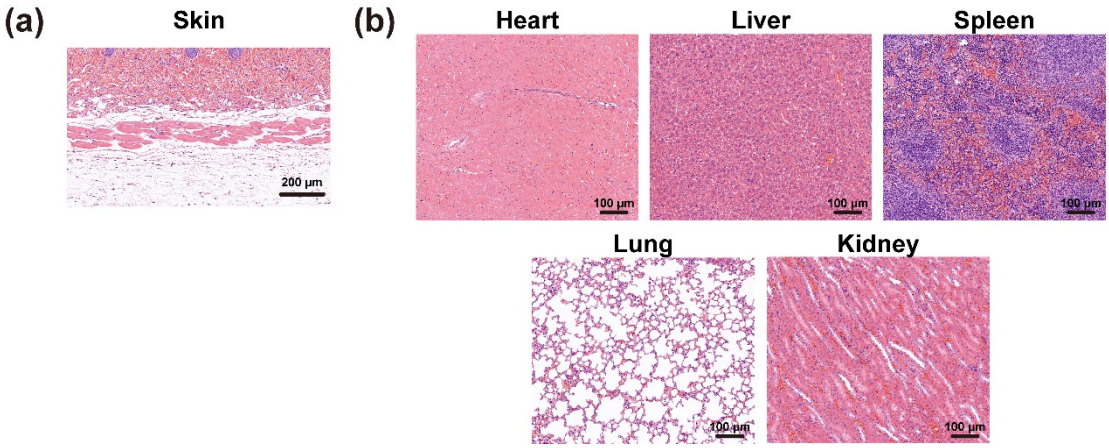

Fig. S12 HE results for the normal skin tissues (a) and organs (b).

References

1 J. Yu, K. Xu, X. J. Chen, X. D. Zhao, Y. X. Yang, D. K. Chu, Y. L. Xu, Q. Zhang, Y. F. Zhang, Y. L. Cheng, *Biomacromolecules*, 2021, **22**, 1297−1304.

2 P. Hohenber, W. Kohn, *Phys. Rev. B*, 1964, **136**, 864-871.

3 P. J. Stephens, F. J. Devlin, C. F. Chabalowski, M. J. Frisch, *J. Phys. Chem.*, 1994, **98** 11623−11627.

4 A. Schaefer, H. Horn, R. Ahlrichs, *J. Chem. Phys.*, 1992, **97**, 2571−77.

5 L. Goerigk, S. Grimme, *J. Chem. Theory Comput.*, 2011, **7**, 291−309.

6 F. Weigend, R. Ahlrichs, *Phys. Chem. Chem. Phys.*, 2005, **7**, 3297−3305.

7 T. Lu, Q.X. Chen, *J. Comput. Chem.*, 2022, **43**, 539−555.

8 S. F. Boys, F. Bernardi, *Mol. Phys.*, 2002, **100**, 65−73.